Large-area, self-healing block copolymer membranes for energy conversion

Christian Sproncken, Peng Liu, Justin Monney, William Fall, Carolina Pierucci, Philip Scholten, Brian van Bueren, Marcos Penedo, Georg Ernest Fantner, Henricus Wensink, et al.

Large area, self-healing block co-polymer membranes for energy conversion

Christian C. M. Sproncken, Peng Liu, Justin Monney, William Stuart Fall, Carolina Pierucci, Philip B. V. Scholten, Brian Van Bueren, Marcos Penedo, Georg Ernest Fantner, Henricus H. Wensink, Ullrich Steiner, Christoph Weder, Nico Bruns, Michael Mayer, Alessandro Ianiro*.*

Abstract

Strongly electric fish continuously convert metabolic energy into electrical potential differences across ion-selective membranes.[1,2] Fabrication of implantable artificial electric organs with this capability will require membranes that are macroscopic, stable, self-healing, fluid, and energy-converting. The work presented here introduces a self-assembly strategy to prepare artificial membranes that meet all these criteria. This strategy uses the interface of an aqueous two-phase system to template and stabilize the formation of molecularly-thin (~35 nm) planar block-copolymer bilayers with scalable areas that can exceed ten square centimeters without defects. These membranes have the ability to self-heal and their barrier function against passage of ions (~1 MΩ cm^2) matches that of phospholipid membranes. The fluidity of these membranes enables straightforward functionalization with molecular carriers that shuttle potassium ions down a concentration gradient with exquisite selectivity over sodium ions. This bioinspired ion-selectivity – in contrast to the charge-selectivity of technical membranes – makes it possible to establish a potential difference across a membrane that separates solutions with equimolar concentrations of NaCl and KCl. We demonstrate applicability by constructing a benchtop prototype artificial electric organ with interconnected fluid reservoirs whose voltage increases by 60 mV with each additional ion-selective membrane stacked in series.

The development of high-performance membranes is key to strategic sectors of the economy and society, as testified by a 6 billion dollars global market in 2021.[3] In the pursuit of new strategies to improve membrane performance, self-assembled biological membranes have often been used as blueprints because of their nanoscale thickness and their ability to regulate with exquisite efficiency and selectivity the exchange of matter within and across living cells.[4,5] In a broad sense, biological membranes and their synthetic counterpart are similar as they both share the function of selective barriers. Yet, biotic membranes outperform abiotic ones in terms of selectivity and permeability.[6] A structural comparison between natural and artificial membranes highlights critical differences that explain this discrepancy in performance. Conventional synthetic membranes are bulk or composite materials with thicknesses of 1-100 µm that act as passive selective barriers thanks to the interplay of chemical composition, porosity, and nanoscale structure. Biological membranes are more sophisticated, as they decouple barrier and transport functions to maximize selectivity and permeability. The barrier function of cell membranes is provided by an extremely thin self-assembled phospholipid bilayer that is virtually impermeable for most hydrophilic and charged molecules. Extreme selectivity is achieved through proteins embedded in the bilayer, which can operate as diffusion-controlled carriers, channels, or chemically-fueled pumps.[4] The molecular-scale thickness of these membranes also contributes to high transport rates for the desired compounds. Permeability, in fact, scales with the inverse of membrane thickness, which hardly exceeds 5 nm in the case of lipid bilayers.[4] Additionally, biological membranes can morph shape without losing functionality because they are held together by dynamic supramolecular interactions providing them with self-healing properties.[5]

Mimicking the intricate design of cell membranes with lipids or amphiphilic block copolymers (BCPs) is a promising route for developing high-performance artificial membranes.[7–11] However, the formation of macroscopic membranes via molecular self-assembly requires control of the self-assembly process across at least 14 orders of magnitude in area (from the molecular scale to the cm^2 and beyond), which thus far could not be achieved by molecular design and with classic self-assembly strategies. Phospholipids, the molecular building blocks of natural membranes, evolved to function best at the cellular length scale while becoming increasingly unstable when assembled across areas that exceed 1 mm^2.[12–14]

Amphiphilic block copolymers represent a versatile synthetic alternative to natural phospholipids because they exhibit similar self-assembly behavior and can form membranes with superior mechanical properties than phospholipids.[10,15–17] However, like natural phospholipids, bilayer-forming BCPs spontaneously assemble into vesicle-like spherical objects rather than flat membranes. Planar BCP membranes can be formed on solid supports by surface-initiated polymerization, vesicle spreading, or by Langmuir monolayer transfer.[10,18,19] Yet, the free-standing areas of such membranes are limited to the square millimeter range[20–23], too small for practical separation or energy conversion applications.

Planar BCP membranes supported by the interface of an aqueous two-phase system

Like many amphiphilic molecules, BCPs accumulate at interfaces because this process minimizes the systems' interfacial energy. We harnessed this thermodynamic driving force to control BCP self-assembly in two dimensions and to stabilize the membrane formed at the interface of two immiscible aqueous solutions. Based on aqueous two-phase systems (ATPS), this approach enables the formation and stabilization of BCP bilayer membranes without blocking access to the membrane for solutes or ions (Figure 1A). An ATPS forms upon bringing two aqueous solutions of chemically incompatible polymers such as poly(ethylene oxide) (PEO) and dextran (DEX) into contact. [24 25–28]

The strategy pursued here is based on the hypothesis that the interface of ATPSs can stabilize planar BCP bilayers (Figure 1A). The interfacial tension (γ) of ATPSs is very small; for the PEO/DEX system investigated here, $\gamma \lesssim 0.1\ \mathrm{mJ \cdot m^{-2}}$, which is 2-3 orders of magnitude lower than the interfacial tension between water and air or water and alkanes.[29] On the molecular scale, such a small interfacial tension does not provide a sufficient driving force for interfacial assembly ($\gamma \lesssim 0.02\ k_\mathrm{B}T \cdot \mathrm{nm^{-2}}$) but, as we demonstrate here, it can provide a significant stabilizing contribution once the membrane is formed (see Supplementary Discussion 1 for thermodynamic details). We used two different BCP types having the same hydrophobic but different hydrophilic blocks that populate the DEX and PEO phases, respectively, so that a compatibilizing asymmetric bilayer can be formed at the interface (Figure 1). Naturally, PEO and DEX are ideal choices for the hydrophilic blocks. However, while PEO-based BCPs are relatively straightforward to prepare[30], DEX is difficult to functionalize selectively, typically has a broad molecular weight distribution, and is almost exclusively soluble in water. Encouraged by previous reports on the use of poly[2-(dimethylamino) ethyl methacrylate] (PDMAEMA) based BCPs to stabilize PEO/DEX water-in-water emulsions[31,32], we selected PDMAEMA as the second hydrophilic block. We tested poly(hexyl methacrylate) and poly(dimethyl siloxane) (PDMS) as a common hydrophobic block for the two block copolymer types. Both hydrophobic blocks enable the formation of large-area ATPS-supported membranes (Supplementary discussion 2), but we chose PDMS for most of the experiments because it is inert, non-toxic, and displays a low glass transition temperature.[33] We expected these characteristics to translate into fluid, self-healing membranes.

We synthesized and characterized BCPs with compositions PEO_{2kDa}-*b*-$PDMS_{5kDa}$ (BCP1) and $PDMAEMA_{2kDa}$-*b*-$PDMS_{5kDa}$ (BCP2) as described in Supplementary Methods and we confirmed their

ability to form planar bilayers using the well-established vertically-folded planar bilayer method [REF] (Supplementary Methods, Extended Data Figure 1 and Supplementary Discussion 2).

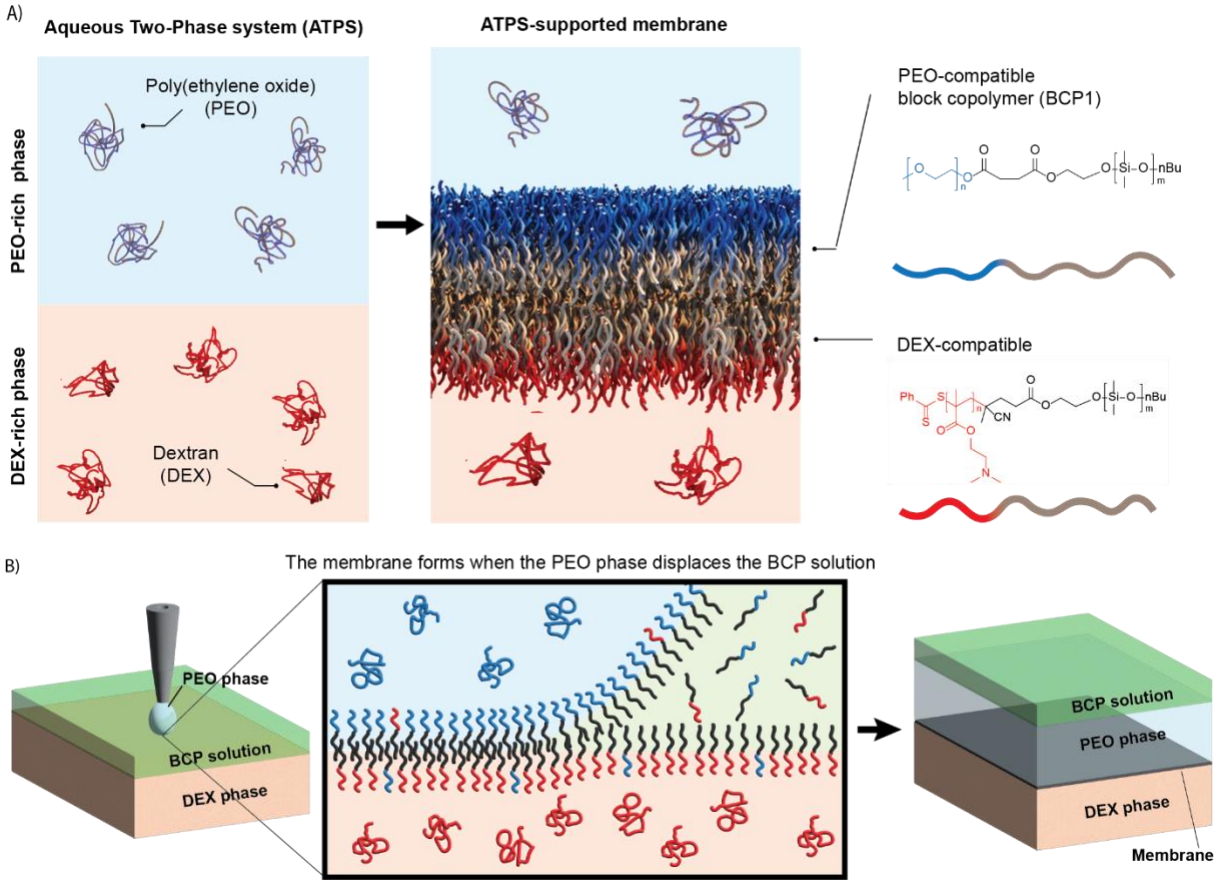

Figure 1. Self-assembly of block copolymer bilayers supported by an aqueous two-phase system (ATPS). A) Schematic representation of an ATPS made of an aqueous solution of poly(ethylene oxide) and an aqueous solution of dextran (left), an ATPS-supported self-assembled bilayer (center), and the two block copolymer types used to form the bilayer (right). B) Schematic description of the solvent displacement method introduced here to form large-area membranes.

Forming membranes with areas larger than $2 \cdot 10^{-3}\ \mathrm{cm}^2$ proved challenging, reflecting that this conventional method for forming planar bilayers is not suitable for the preparation of macroscopic membranes.

As the low interfacial tension of the ATPS does not provide a sufficient driving force at the molecular scale to guide interfacial assembly, we devised a two-step templating strategy that is based on the displacement of a water-immiscible organic solvent from the interface of the two aqueous phases (Figure 1B). We added the DEX solution, which is denser than the PEO solution, to a vessel whose cross-section defines the area of the membrane. Then, we gently placed a solution of the two BCPs in a suitable organic solvent on top of the DEX phase (Figure 1B). It is well known that in these conditions a BCP monolayer forms at the interface between the aqueous and the organic phases [REF]. The monolayer is richer in BCP2 than BCP1, as demonstrated by FRET measurements and computer simulations (Supplementary discussion 3-5 and Figure 2 C) because interactions between DEX and the PEO blocks of BCP1 are enthalpically unfavorable. Finally, we slowly added the aqueous PEO phase from the top. This phase is denser than the organic solvent and sinks towards the DEX phase, thereby

displacing the organic solvent, which rises to the top. During this displacement process, a second monolayer, richer in BCP1 than BCP2 (Supplementary discussion 3-5 and Figure 2 C), forms at the interface between the organic phase and the PEO solution. When the PEO and DEX phases meet, the two monolayers merge into a planar BCP bilayer (Figure 1B).

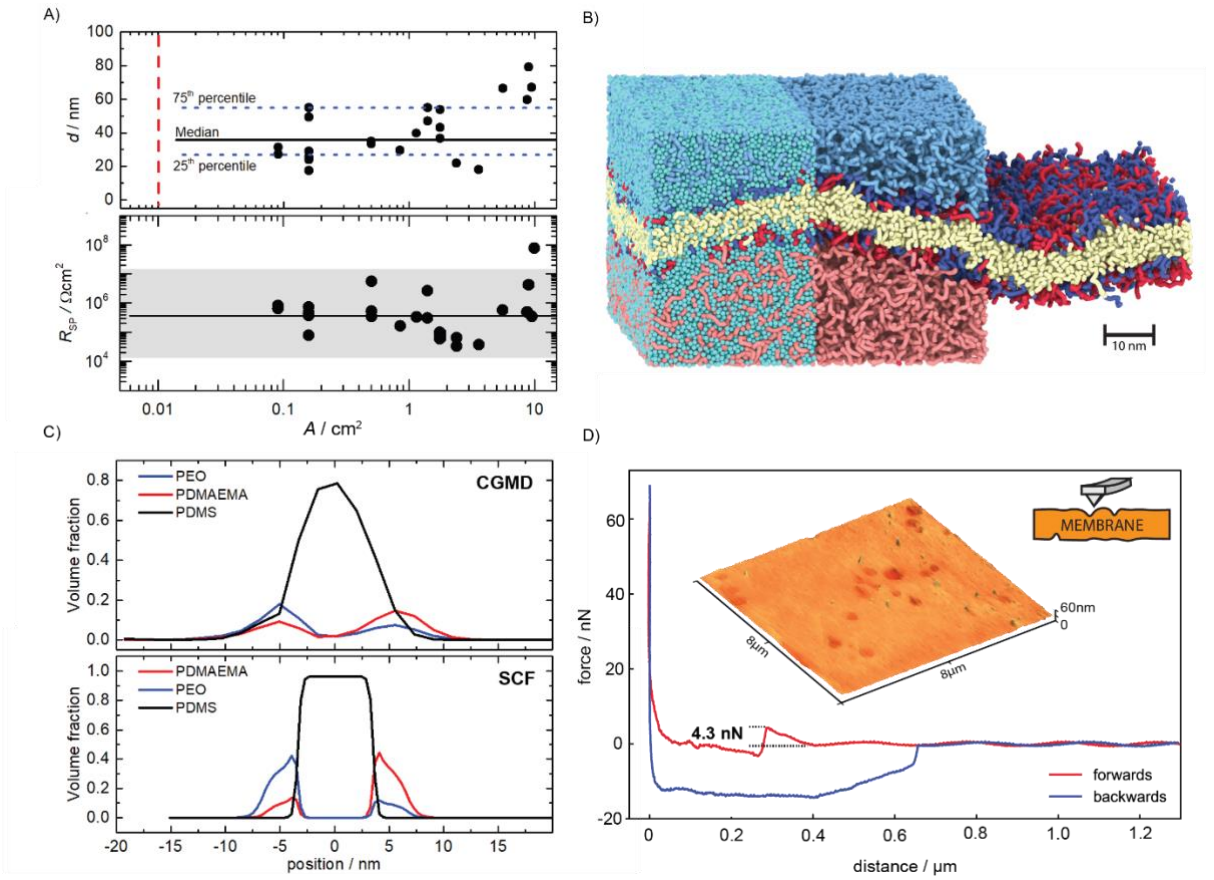

Figure 2. Experimental cand theoretical characterization of ATPS-supported membranes. A) Membrane thickness (d) from capacitive measurements and specific electric resistance (R_{SP}) for membranes with different surface areas (A); each black dot corresponds to a single membrane. In the top panel, the black horizontal line is the median d value while the blue dotted lines indicate the first and third quartile; the red dashed vertical line indicates the area of the largest self-assembled BCP membrane reported in the literature[23]; the grey region in the bottom panel indicates the reference range of R_{SP} values for lipid bilayers.[35–37] B) Structure of an ATPS-supported membrane resulting from coarse-grained molecular dynamics (CGMD) simulations. The CGMD snapshot is divided in three segments. The left segment displays the full composition of the ATPS interface when a membrane is formed, with water (cyan) PEO homopolymers (light blue), DEX (light red), PEO blocks (dark blue) PDMAEMA blocks (dark red) and PDMS (cream). The central segment shows only the block copolymers and the homopolymers while the right segment displays only the ATPS-supported bilayer. C) Concentration profiles describing the composition of the bilayer in the direction perpendicular to the membrane plane obtained via CGMD simulations (top) and self-consistent field (SCF) computations (bottom). Both CGMD and SCF predict the formation of asymmetric bilayers. D) Atomic force microscopy (AFM) characterization of the ATPS-supported membranes. The red and blue curves represent cantilever force versus tip-sample distance in the forward and backward directions. The abrupt change on the red force curve at 0.3 µm distance represent the penetration of the membrane, from which we obtained a penetration force of 4.3 nN. The darker regions on the membrane plane represent small variations in the membrane thickness of approximately 6 nm (Supplementary Figure 1), and hence much smaller than the total membrane thickness (~40 nm for this membrane) determined via capacitive measurements.

This approach has elements in common with the droplet interface bilayer method[41], in which two aqueous droplets, coated by lipid monolayers upon immersion in an oil-lipid mixture, are brought into contact to form a bilayer. The solvent displacement method, however, introduces the concept of forming and stabilizing macroscopic self-assembled membranes by minimizing the interfacial free energy of an aqueous two-phase system. This concept is realized by selecting block-copolymers with hydrophilic blocks that are compatible with the aqueous phase on either side of the membrane. Application of the solvent displacement method using two PEO solutions as phase 1 and phase 2 together with BCP1 or two DEX solutions together with BCP2 did not result in the formation of stable membranes, confirming the essential stabilizing role of the ATPS interface (Supplementary Discussion 2).

We applied the solvent displacement method using various water-immiscible organic solvents (Supplementary Discussion 6). Of the six solvents we tested, only those with viscosities $\eta > 0.5$ mPa·s such as toluene, yielded stable membranes; Supplementary Discussion 6 provides an interpretation of this unexpected dependence on the solvent viscosity. We selected toluene for most of the subsequent studies because it is commonly available and broadly used in polymer science. The water/toluene interface is sharp and characterized by an interfacial tension of $\gamma \approx 35\ \mathrm{mJ \cdot m^{-2}}$ ($\gamma \approx 8\ k_\mathrm{B}T \cdot \mathrm{nm^{-2}}$)[39], which provides a strong driving force for the assembly of monolayers.

The solvent displacement method introduced here made it possible to form ATPS-stabilized membranes with surface areas of $10\ \mathrm{cm^2}$. These membranes are three orders of magnitude larger than the largest bilayers produced with the folding method[40] and, to our knowledge, the largest free-standing self-assembled bilayers reported to date. Without a notable dependence on the surface area, the ATPS-stabilized membranes displayed a median thickness of $d \cong 35\ \mathrm{nm}$ (Figure 2A), a specific electrical resistance exceeding $0.1\ \mathrm{M\Omega \cdot cm^2}$ (similar to lipid bilayers, Figure 2A), and a stability for several hours (sometimes exceeding 12 h) before spontaneously breaking.

Supplementary discussions 3-5 provide an extensive experimental and theoretical characterization of the ATPS-supported membranes. For instance, fluorescence resonance energy transfer (FRET) experiments confirm that the membranes are indeed asymmetric, with the two block copolymers partitioning in different proportions to the two sides of the bilayer as hypothesized for the proposed membrane formation mechanism (Figure 1). Coarse-grained molecular dynamics (CGMD) simulations (Figure 2B-C) and self-consistent field computations (Figure 2C) support this experimental result. The mechanical properties of these large-area ATPS-stabilized membranes are comparable to those of the cell membrane [Marcos Penedo et al. ,Visualizing intracellular nanostructures of living cells by nanoendoscopy-AFM.Sci. Adv.7,eabj4990(2021).DOI:10.1126/sciadv.abj4990; Nano Lett. 2009, 9, 6, 2501–2507 Publication Date:May 19, 2009 https://doi.org/10.1021/nl901384x] with a penetration force measured by atomic force microscopy (AFM) of approximately 4 nN (Figure 2D). Moreover, the membranes can withstand osmotic pressure differences up to 4 kPa, above which defects start to form. Moreover, the ATPS-supported membranes provide an excellent barrier function towards the passage of charged organic dyes (Figure 3 A) and possess the ability to self-heal from repeated mechanical damages over a length scale that is 3000 times larger than their thickness, as explained in Figure 3 B-C. Simulations by CGMD confirm the self-healing capability of the membranes (Supplementary Video 1) and provide an estimate of the in-plane diffusion coefficient of the BCPs $D \approx 1.7 \times 10^{-6}$ $\mathrm{cm^2 \cdot s^{-1}}$. This value, which is comparable to the diffusion coefficient of lipids in biotic membranes [refs], corroborates that the ATPS-supported membranes are fluid.

Enabling selective transport in ATPS membranes: towards biomimetic electric power generation

Biological membranes are more than barriers, as they control the transport of specific compounds with unique selectivity and efficiency. We imparted the same functionality to the ATPS-supported large-area membranes by incorporating the selective ion transporter valinomycin (Figure 4A), which is a naturally occurring cyclic hydrophobic peptide bearing a K^+-selective binding pocket. Its hydrophobicity

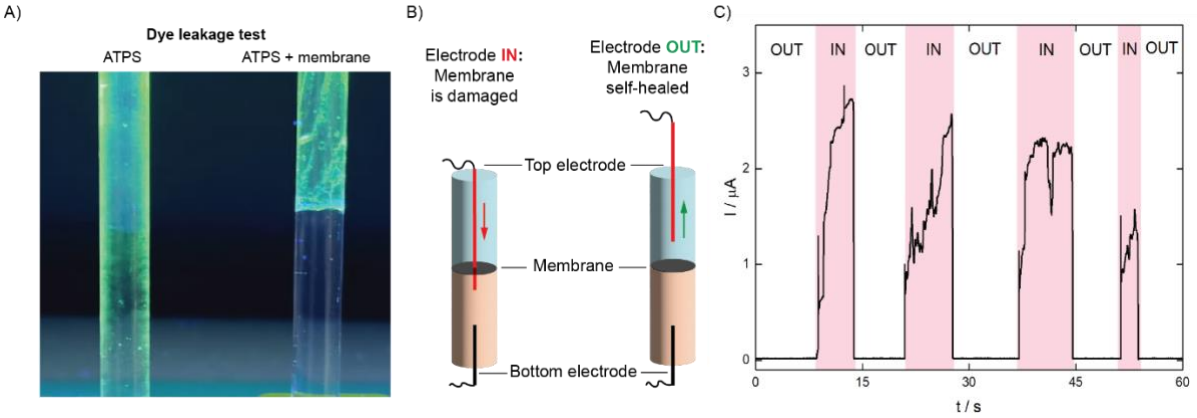

Figure 3. Self-healing properties of the ATPS-supported membranes. A) Dye leakage test showing that a membrane at an ATPS interface can block the diffusion of the negatively charged dye calcein that was added to the PEO phase. The photograph shows glass cylinders with an inner diameter of 6 mm under UV light after 2 h of sample preparation at room temperature. B) Schematic representation of the self-healing test plotted in panel C). We measured the current across a membrane via two Ag/AgCl electrodes at a constant applied potential of 100 mV. Initially the two electrodes are far from the membrane (OUT) and the transmembrane current is negligible, indicating that the membrane has no defects. Subsequently we lowered the top electrode, with a cross-sectional diameter of 100 µm (approximately 3000 times the membrane thickness), using a precision linear positioner until it perforates the membrane (IN) leading to a sudden current jump. When we retracted the electrode (OUT) the current went back to zero, demonstrating that the damage inflicted by the electrode was repaired. We repeated the test four times to show that the membrane can heal from repeated damage.

promotes the accumulation within the hydrophobic core of the membrane, where it can freely diffuse and shuttle K^+ ions to equilibrate transmembrane concentration gradients. We first explored and confirmed the incorporation of valinomycin on small-scale BCP membranes made of BCP1 and BCP2 obtained via the conventional folding method (Extended Data Figure 2). Subsequently, we incorporated valinomycin into ATPS-supported membranes by adding it to the solution of BCPs in toluene. We modified the ATPS to introduce an ion concentration gradient across the membrane (Figure 4A) by using KCl (500 mM) as an electrolyte in the DEX phase and NaCl (390 mM to achieve osmotic matching of the phases) in PEO phase. The gradient thus produced is like the one across the plasma membrane of living cells (albeit with higher ion concentrations) and is expected to yield a transmembrane potential if selective ion transport occurs (Supplementary Discussion 7).

We tested various molar ratios of valinomycin to BCPs and found that the incorporation of valinomycin causes a progressive reduction of the membrane electrical resistance and the appearance of potential and current offsets (Figure 4 B-D). The potential offset $V(I = 0)$ or open circuit voltage (V_{oc}) is the transmembrane equilibrium potential, while the offset current $I(V = 0)$, referred to as I_0, is a measure of the net flux of charges across the membrane driven by the concentration gradient. Figure 4C plots values of I_0 obtained from electrical measurements.

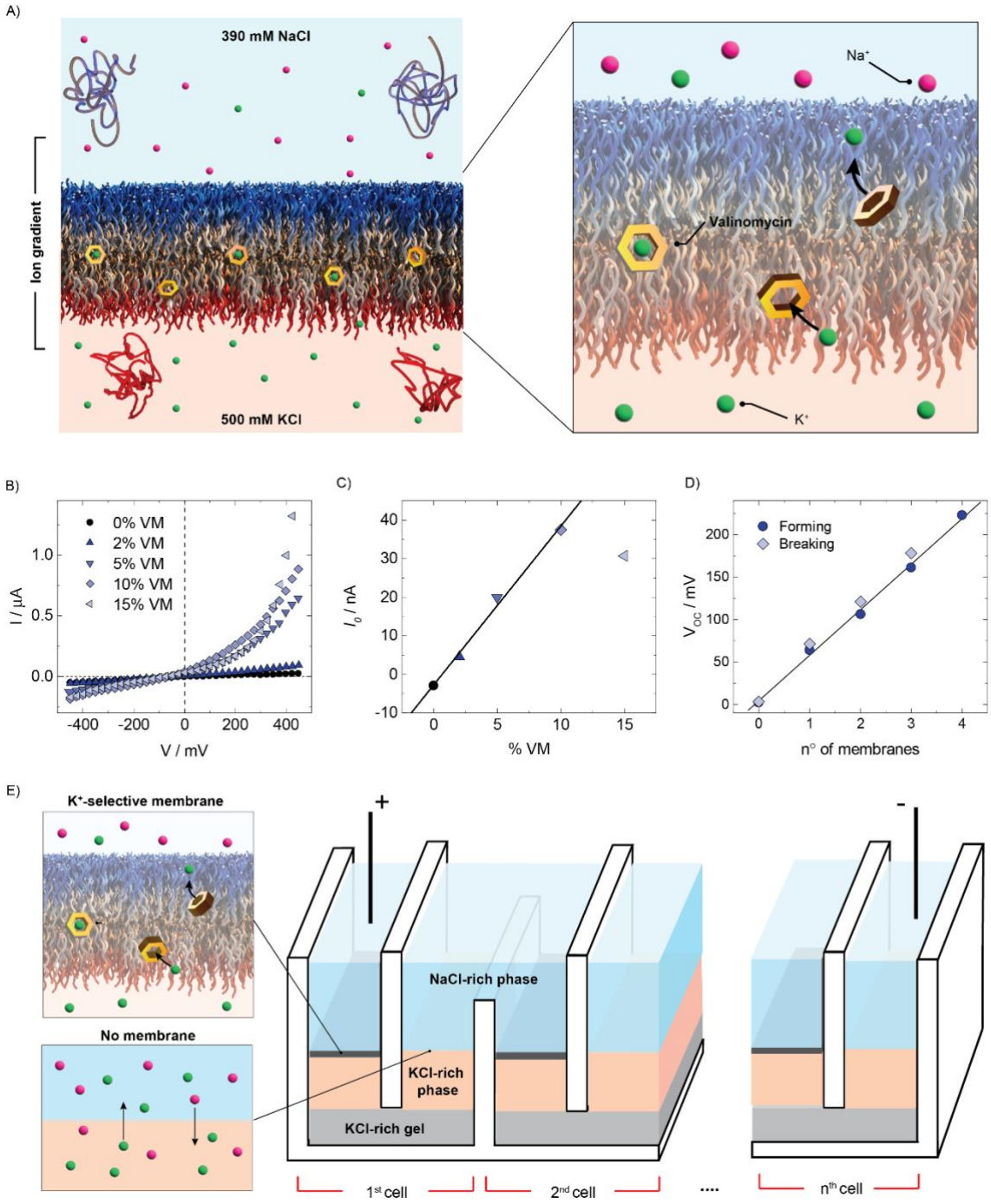

Figure 4. Electrical power generation by ATPS-supported ion-selective membranes. A) Schematic of the valinomycin-doped membranes showing the selective K^+ transport mechanism; valinomycin (VM) is represented as a yellow hexagon. B) Current-potential (I-V) curves for membranes prepared with different VM:BCP molar ratios. C) Currents (I_0) extracted from the I-V curves in B) for potentials $V = 0$ mV. D) Open circuit voltage V_{oc} of the device inspired by electric rays as a function of the number of membranes doped with 5 mol % VM. Dark blue markers and linear fits represent increases of the potential difference upon membrane formation. Light blue markers represent potential drops upon intentional membrane disruption. E) Schematic drawing of the electric-ray-inspired power unit with stacks of ion selective membranes developed in this work.

The incorporation of valinomycin leads to a linear I_0 increase up to a valinomycin to block copolymer molar ratio of 10%, while incorporation of more valinomycin yields no I_0 increase and impacts membrane stability negatively, suggesting that valinomycin aggregates in the membrane above 10% molar ratio. These measurements demonstrate that the ATPS-supported BCP membranes presented here are fluid, as ionophores can freely diffuse in their hydrophobic core to shuttle ions, and that they can be transformed into macroscopic ion-selective membranes.

Ion selectivity is very difficult to achieve in bulk materials. In contrast, most commercial membranes are selective only to charge (anions versus cations), but unlike charge selectivity, ion selectivity allows to convert energy from isotonic ion gradients (e.g., 1 M KCl/1 M NaCl). Quasi-isotonic NaCl/KCl gradients are ubiquitous in biology, as sodium-potassium pumps maintain the cell environment rich in KCl and expel NaCl to the extracellular space. Interestingly, the Atlantic torpedo (*Tetronarce nobiliana)*, a species of electric ray, uses ion selectivity to convert such gradients into electric discharges of up to 1 kW power.[42] This fish evolved plate-like cells (electrocytes) that behave like a small battery thanks to a special enervated membrane.[42] The membrane at one side of the cell can generate a potential by opening selective ion channels on-demand. The opposite side does not contribute to the potential but has a low resistance to ensure a large ionic current flow. Stacking electrocytes in series and parallel allows torpedo rays to produce biology's most powerful potentials and current output (see schematic in Supplementary Figure 2).

Inspired by the torpedo ray, we designed a small electric power generator that takes advantage of the planar nature of large ATPS-stabilized membranes and the unique features of an ATPS and to stack multiple ion-selective membranes in series. As shown in Figure 4E, the fundamental unit of the device consists of two ATPSs ionically connected via the DEX (+ 500 mM KCl) phases through a KCl-rich hydrogel bridge (Supplementary Methods). The hydrogel ensures high conductivity and prevents hydrostatic mismatch of communicating vessels. We formed a valinomycin-doped BCP membrane (with a diameter of 6 mm) at one of the two interfaces with the solvent displacement method, while we didn't form a membrane at the other interface to facilitate the free passage of ions (Figure 4E). These two interfaces imitate the two sides of torpedo rays' electrocytes. Figure 4D shows that membrane potentials become additive when several fundamental units are connected via the PEO phases and that the V_{oc} of the device scales linearly with the number of membranes. Each additional unit contributes to the overall potential difference with approximately $60\ \mathrm{mV}$, similar to the potential generated by the torpedo's electrocytes, although larger potentials were obtained in some attempts (Extended Data Figure 3). Intentionally breaking the membranes mechanically caused a step-wise drop of potential difference, with reductions by approximately 60 mV. This observation confirms that the potential difference of the device originates from additive transmembrane potentials. By solving the Goldman–Hodgkin–Katz (GHK) equation[43,44], which relates V_{oc} to ion concentrations and membrane permselectivity for the various ionic species, we determined that the valinomycin-doped membrane is approximately eight times more permselective for K^+ than for Na^+ (Supplementary Discussion 7), in line with previous reports.[45]

The device was not optimized for power output (power density per membrane $PD \approx 0.04\ \mathrm{mW \cdot m^{-2}}$) because K^+ transport mediated by valinomycin is not efficient, as testified by the small I_0 values in Figure 4C. In the future, the use of natural or synthetic ion channels, which can be 100- to 1000-fold more efficient in transporting ions than valinomycin [46–49], may enhance device performance up to that of the electric ray ($PD \approx 28\ \mathrm{W \cdot m^{-2}}$).[42]

The approach presented here introduces the concept of using aqueous two-phase systems to control the self-assembly of BCPs into planar free-standing bilayer membranes with areas of previously inaccessible sizes. It enables the formation of stable, macroscopic (cm^2), molecularly-thin, self-healing

and fluid membranes that can incorporate molecular carriers. Since block copolymer membranes have been used for reconstitution of functional transmembrane proteins,[50] the final step for fabricating stable, large-area, ion-selective membranes that convert chemical energy into differences in electrical potential can now be envisaged. The planar nature of these membranes makes it possible to stack them in series in order to reach desired potential differences. These macroscopic membranes may also find application in electrophysiology and other biophysical characterization methods of membrane proteins such as X-ray or neutron reflectivity. Finally, these membranes may enable high-value separations, blue power generation, and the preparation of ion-selective membranes for fuel cells.

Methods

Electric characterization of self-assembled membranes

The electric behavior of self-assembled bilayers is described by an equivalent circuit that consists of a resistor and capacitor in parallel.[34] The resistive part describes the ability of the bilayer to hinder the passage of ions and therefore quantifies its barrier function. The capacitive element is related to the hydrophobic core of the bilayer, which acts as a dielectric material between two conductive regions, similar to a plate capacitor. The behavior of such a system is described by

$$I = A\left[\frac{V}{R_{\mathrm{SP}}} + \left(\frac{\varepsilon\varepsilon_0}{d} - \frac{C_{\mathrm{S}}}{A}\right)\frac{\mathrm{d}V}{\mathrm{d}t}\right], \qquad (1)$$

where I [A] is the current across the bilayer, V $[V]$ is the applied potential, ε_0 is the vacuum permittivity, t [s] is the time, C_{S} [F] is the capacitance of the setup excluding the membrane, A [m^2] is the area of the bilayer, d [m] is the thickness of the hydrophobic core, R_{SP} $[\Omega]$ is the specific resistance of the membrane and ε is the relative dielectric constant of the hydrophobic core. According to equation 1, d and R_{SP} can be determined from electric measurements applying time-varying potentials. We used a value of 2.7 for ε.[REF]

An e2HC amplifier from Elements Srl (Italy) connected to two Ag/AgCl electrodes was used to measure currents across the membranes in response to applied voltage protocols. The system was placed on an anti-vibration table inside a Faraday cage to prevent electrostatic and vibrational noise to affect the measurements. The e2HC amplifier makes it possible to apply square-wave voltage protocols to determine R_{SP} and triangular-wave voltage protocols to determine d independently. When the bilayer folding setup was used, the capacitance of the setup C_{S} was determined by putting a Teflon partition without hole between the two chambers filled with electrolyte solution. The measured capacitance was C_{S} =25 pF and this value was deducted for all the measurements of the membranes. Contrarily, the capacitance of the ATPS setup was neglected because it is much smaller than the capacitance of the formed bilayer ($\varepsilon\varepsilon_0/d \gg C_{\mathrm{S}}/A$). All recordings have been analyzed with a custom-made Python code to determine R_{SP} and d.

Solvent displacement method for the formation of large-area membranes

The block copolymer (BCP) membranes supported by an aqueous two phase system (ATPS) were formed using osmotically matched solutions of poly(ethylene oxide) (PEO), dextran (DEX) and salt. For a system containing only one type of salt (NaCl), 197 mg·mL^{-1} DEX and 120 mg·mL^{-1} PEO were dissolved

in a 1 M NaCl solution. The phase-separated mixture was left to equilibrate overnight, after which the two phases were isolated by means of a separation funnel. For an ATPS with two types of salt (NaCl in the PEO phase and KCl in the DEX phase), the osmolality of 197 mg·mL^{-1} DEX in 0.5 M KCL was measured (885 mOsm·kg^{-1}) and the osmotically matching NaCl concentration (0.39 M) for the 120 mg·mL^{-1} PEO solution was determined from a calibration curve (see Supplementary Methods and Supplementary Figure 3 for details).

To construct the membrane, a containing vessel such as a glass Pasteur pipet with 4.5 mm internal diameter cut to few cm in length, was closed at the bottom with a rubber plug wherein an Ag/AgCl wire electrode was embedded. Then, 0.5 mL of DEX/salt solution were pipetted into the glass cylinder, followed by the addition of 50 µL of BCP solution in toluene. The mass concentration of each of the two BCPs was 25 mg·mL^{-1}, hence the total BCP concentration was 50 mg·mL^{-1}. After 5 min, 0.5 mL of PEO/salt solution was injected with a syringe and needle, just below the surface of the toluene solution, near the side of the glass wall. This gentle injection expelled the toluene to the top, producing a polymer membrane at the newly formed PEO/DEX interface. Excess toluene was removed from the top and a second Ag/AgCl wire electrode was inserted in the top phase. The electrodes were connected to the amplifier to characterize the membrane. Other glass containers with different diameters (D_{int}) that were used, to assess membranes with smaller and larger areas, were NMR tubes (D_{int} = 3.4 mm) and various types of culture tubes (D_{int} = 8.0, 10.4, 13.4 mm). To further extend the membrane area we 3D printed containers with a straight channel and with a spiraling channel (Figure 3 A and Extended Data Figure 4). The internal width of these channels was 5 mm and the bottom of these containers was slanted, so that the membrane area could be tuned by depositing less or more of the DEX solution in the bottom. Wire electrodes were inserted from the bottom at the deepest end and the counter electrodes were submerged in the PEO solution from the top after membrane assembly. The slanted bottom of the containers enabled to gently expel the excess toluene solution when injecting the PEO top solution from the higher part of the slanted bottom. We also tested containers with internal pillars to support the membrane, which enabled us to form membranes with surface-area exceeding 10 cm^2 (Extended data Figure 4).

Incorporation of Valinomycin into the block copolymer membranes

To incorporate valinomycin into the BCP membranes, a stock solution was prepared containing 25 mg·mL^{-1} of each block copolymer and 1.8 mg·mL^{-1} of valinomycin (1.62 mM, 20 mol% with respect to the total amount of BCP) in toluene. To obtain the desired final concentration of valinomycin, this stock solution was mixed in the corresponding ratio with a BCP solution without any valinomycin. To check the incorporation and function of valinomycin in the membranes, the planar bilayer setup (with 110 µm aperture) was again used, this time having DEX/KCl and PEO/NaCl solutions in the respective chambers rather than equimolar KCl solutions (Extended Data Figure 3). Large-area membranes containing valinomycin were then formed with the solvent displacement method using valinomycin-containing BCP solutions in toluene. I-V curves were recorded by stepwise increasing or decreasing the voltage between -500 and +500 mV with steps of 25 mV. Each step was recorded for a duration of 5 s, but the corresponding current value was determined by discarding the first 500 ms of the step as they are affected by capacitive currents induced by the stepwise potential change.

Data Availability

The data supporting the findings reported in this work are available in Zenodo (https://zenodo.org/) with open access right (DOI: 10.5281/zenodo.7818212)

Code Availability

The python code used of the data analysis is available in Zenodo (https://zenodo.org/) with open access right (DOI: 10.5281/zenodo.7818212)

REFERENCES

1. Schroeder, T. B. H. *et al.* An electric-eel-inspired soft power source from stacked hydrogels. *Nature* **552**, 214–218 (2017).
2. Guha, A. *et al.* Powering Electronic Devices from Salt Gradients in AA-Battery-Sized Stacks of Hydrogel-Infused Paper. *Advanced Materials* **33**, 2101757 (2021).
3. Membranes Market Size, Share, Growth | Forecast Report, 2029. https://www.fortunebusinessinsights.com/membranes-market-102982.
4. Gennis, R. B. *Biomembranes*. (Springer New York, 1989). doi:10.1007/978-1-4757-2065-5.
5. Alberts, B. *et al. Molecular Biology of the Cell, 4th edition*. (Garland Science, 2002).
6. Pusch, W. Efficiency of synthetic membranes in comparison with biological membranes. *Desalination* **62**, 5–18 (1987).
7. Gouveia, M. G. *et al.* Polymersome-based protein drug delivery – quo vadis? *Chem Soc Rev* **52**, 728–778 (2023).
8. Rideau, E., Dimova, R., Schwille, P., Wurm, F. R. & Landfester, K. Liposomes and polymersomes: a comparative review towards cell mimicking. *Chem Soc Rev* **47**, 8572–8610 (2018).
9. Peters, R. J. R. W., Louzao, I. & van Hest, J. C. M. From polymeric nanoreactors to artificial organelles. *Chem. Sci.* **3**, 335–342 (2012).
10. Palivan, C. G. *et al.* Bioinspired polymer vesicles and membranes for biological and medical applications. *Chem Soc Rev* **45**, 377–411 (2016).
11. Renggli, K. *et al.* Selective and Responsive Nanoreactors. *Adv Funct Mater* **21**, 1241–1259 (2011).
12. Beltramo, P. J., Scheidegger, L. & Vermant, J. Toward Realistic Large-Area Cell Membrane Mimics: Excluding Oil, Controlling Composition, and Including Ion Channels. *Langmuir* **34**, 5880–5888 (2018).
13. Beltramo, P. J., Van Hooghten, R. & Vermant, J. Millimeter-area, free standing, phospholipid bilayers. *Soft Matter* **12**, 4324–4331 (2016).
14. Ryu, H., Fuwad, A., Kim, S. M. & Jeon, T.-J. Multilayered film for the controlled formation of freestanding lipid bilayers. *Colloids Surf B Biointerfaces* **199**, 111552 (2021).
15. Lee, J. C.-M., Santore, M., Bates, F. S. & Discher, D. E. From Membranes to Melts, Rouse to Reptation: Diffusion in Polymersome versus Lipid Bilayers. *Macromolecules* **35**, 323–326 (2002).
16. Du, J. Polymer Vesicles. in *Advanced Hierarchical Nanostructured Materials* (eds. Qiang Zhang & Wei Fei) (Wiley, 2014).

17. Discher, D. E. & Eisenberg, A. Polymer Vesicles. *Science (1979)* **297**, 967–973 (2002).

18. Puiggalí-Jou, A., del Valle, L. J. & Alemán, C. Biomimetic hybrid membranes: incorporation of transport proteins/peptides into polymer supports. *Soft Matter* **15**, 2722–2736 (2019).

19. Belegrinou, S. *et al.* Biomimetic supported membranes from amphiphilic block copolymers. *Soft Matter* **6**, 179–186 (2010).

20. Chimisso, V., Maffeis, V., Hürlimann, D., Palivan, C. G. & Meier, W. Self-Assembled Polymeric Membranes and Nanoassemblies on Surfaces: Preparation, Characterization, and Current Applications. *Macromol Biosci* **20**, 1900257 (2020).

21. Kowal, J., Zhang, X., Dinu, I. A., Palivan, C. G. & Meier, W. Planar Biomimetic Membranes Based on Amphiphilic Block Copolymers. *ACS Macro Lett* **3**, 59–63 (2014).

22. Zhang, X., Tanner, P., Graff, A., Palivan, C. G. & Meier, W. Mimicking the cell membrane with block copolymer membranes. *J Polym Sci A Polym Chem* **50**, 2293–2318 (2012).

23. Nardin, C., Winterhalter, M. & Meier, W. Giant Free-Standing ABA Triblock Copolymer Membranes. *Langmuir* **16**, 7708–7712 (2000).

24. Sargantanis, I. G. & Karim, M. N. Prediction of Aqueous Two-Phase Equilibrium Using the Flory−Huggins Model. *Ind Eng Chem Res* **36**, 204–211 (1997).

25. Grilo, A. L., Raquel Aires-Barros, M. & Azevedo, A. M. Partitioning in Aqueous Two-Phase Systems: Fundamentals, Applications and Trends. *Separation & Purification Reviews* **45**, 68–80 (2016).

26. Asenjo, J. A. & Andrews, B. A. Aqueous two-phase systems for protein separation: A perspective. *J Chromatogr A* **1218**, 8826–8835 (2011).

27. Iqbal, M. *et al.* Aqueous two-phase system (ATPS): an overview and advances in its applications. *Biological Procedures Online 2016 18:1* **18**, 1–18 (2016).

28. Hann, S. D., Lee, D. & Stebe, K. J. Tuning interfacial complexation in aqueous two phase systems with polyelectrolytes and nanoparticles for compound all water emulsion bodies (AWE-somes). *Physical Chemistry Chemical Physics* **19**, 23825–23831 (2017).

29. Ryden, J. & Albertsson, P. Interfacial tension of dextran—polyethylene glycol—water two—phase systems. *J Colloid Interface Sci* **37**, 219–222 (1971).

30. Kutikov, A. B. & Song, J. Biodegradable PEG-Based Amphiphilic Block Copolymers for Tissue Engineering Applications. *ACS Biomater Sci Eng* **1**, 463–480 (2015).

31. Buzza, D. M. A., Fletcher, P. D. I., Georgiou, T. K. & Ghasdian, N. Water-in-Water Emulsions Based on Incompatible Polymers and Stabilized by Triblock Copolymers–Templated Polymersomes. *Langmuir* **29**, 14804–14814 (2013).

32. Inam, M. *et al.* Controlling the Size of Two-Dimensional Polymer Platelets for Water-in-Water Emulsifiers. *ACS Cent Sci* **4**, 63–70 (2018).

33. Wolf, M. P., Salieb-Beugelaar, G. B. & Hunziker, P. PDMS with designer functionalities—Properties, modifications strategies, and applications. *Prog Polym Sci* **83**, 97–134 (2018).

34. Hanke, W. & Schlue, W.-R. *Planar Lipid Bilayers*. (Elsevier, 1993). doi:10.1016/C2009-0-03331-5.

35. Montal, M. & Mueller, P. Formation of Bimolecular Membranes from Lipid Monolayers and a Study of Their Electrical Properties. *Proceedings of the National Academy of Sciences* **69**, 3561–3566 (1972).

36. Winterhalter, M. Black lipid membranes. *Curr Opin Colloid Interface Sci* **5**, 250–255 (2000).

37. Naumowicz, M., Petelska, A. D. & Figaszewski, Z. A. Capacitance and resistance of the bilayer lipid membrane formed of phosphatidylcholine and cholesterol. *Cell Mol Biol Lett* **8**, 5–18 (2003).

38. White, S. H., Petersen, D. C., Simon, S. & Yafuso, M. Formation of planar bilayer membranes from lipid monolayers. A critique. *Biophys J* **16**, 481–489 (1976).

39. Sun, Z., Feng, T. & Russell, T. P. Assembly of Graphene Oxide at Water/Oil Interfaces: Tessellated Nanotiles. *Langmuir* **29**, 13407–13413 (2013).

40. Nardin, C., Winterhalter, M. & Meier, W. Giant Free-Standing ABA Triblock Copolymer Membranes. *Langmuir* **16**, 7708–7712 (2000).

41. Bayley, H. *et al.* Droplet interface bilayers. *Mol Biosyst* **4**, 1191 (2008).

42. Bennett, M. V. L., Wurzel, M. & Grundfest, H. The Electrophysiology of Electric Organs of Marine Electric Fishes. *Journal of General Physiology* **44**, 757–804 (1961).

43. Bowman, C. L. & Baglioni, A. Application of the Goldman-Hodgkin-Katz current equation to membrane current-voltage data. *J Theor Biol* **108**, 1–29 (1984).

44. Yamaguchi, T., Kitazumi, Y., Kano, K. & Shirai, O. Permselectivity of Gramicidin A Channels Based on Single-channel Recordings. *Electroanalysis* **32**, 1093–1099 (2020).

45. Andreoli, T. E., Tieffenberg, M. & Tosteson, D. C. The Effect of Valinomycin on the Ionic Permeability of Thin Lipid Membranes. *Journal of General Physiology* **50**, 2527–2545 (1967).

46. Martin, M., Dubbs, T. & Fried, J. R. Planar Bilayer Measurements of Alamethicin and Gramicidin Reconstituted in Biomimetic Block Copolymers. *Langmuir* **33**, 1171–1179 (2017).

47. Barboiu, M. *et al.* An artificial primitive mimic of the Gramicidin-A channel. *Nat Commun* **5**, 4142 (2014).

48. Mayer, M., Kriebel, J. K., Tosteson, M. T. & Whitesides, G. M. Microfabricated Teflon Membranes for Low-Noise Recordings of Ion Channels in Planar Lipid Bilayers. *Biophys J* **85**, 2684–2695 (2003).

49. Yu, L. *et al.* Stable polymer bilayers for protein channel recordings at high guanidinium chloride concentrations. *Biophys J* **120**, 1537–1541 (2021).

50. Garni, M., Thamboo, S., Schoenenberger, C. A. & Palivan, C. G. Biopores/membrane proteins in synthetic polymer membranes. *Biochimica et Biophysica Acta - Biomembranes* vol. 1859 619–638 Preprint at https://doi.org/10.1016/j.bbamem.2016.10.015 (2017).

Acknowledgments

This work was financially supported by the National Centre for Competence in Research (NCCR) Bioinspired Materials, a research instrument of the Swiss National Science Foundation (SNSF), by the Pathfinder Open project INTEGRATE (grant number 101046333) co-financed by the European Innovation Council (EIC) and the Swiss State Secretariat for Education, Research and Innovation (SERI), and by and the Adolphe Merkle Foundation. M. P. was supported by the H2020 - UE Framework Programme for Research & Innovation (2014-2020), ERC-2017-CoG, InCell, Project number 773091. The authors thank Dr. P. Molet Bachs for help with the CAD drawings of the 1D extended vessels. W.S.F wishes to thank Prof Jörg Baschnagel and Dr Hendrik Meyer for helpful discussions and comments on manuscript preparation.

This work was granted access to the HPC resources of IDRIS under the allocation 20*XX-[numéro de dossier]* made by GENCI

Author information

Authors and affiliation

University of Fribourg, Adolphe Merkle Institute, Chemin des Verdiers 4, 1700, Fribourg, Switzerland

Christian C. M. Sproncken, Peng Liu, Justin Monney, Carolina Pierucci, Philip B. V. Scholten, Brian Van Bueren, Ulrich Steiner, Christoph Weder, Michael Mayer, Alessandro Ianiro.

Swiss National Center for Competence in Research (NCCR) Bio-inspired Materials, University of Fribourg , Chemin des Verdiers 4, CH-1700 Fribourg, Switzerland

Christian C. M. Sproncken, Peng Liu, Carolina Pierucci, Ulrich Steiner, Christoph Weder, Michael Mayer, Alessandro Ianiro.

Department of Chemistry, Technical University of Darmstadt, Alarich-Weiss-Straße 4, 64287 Darmstadt, Germany

Nico Bruns

Division of Chemistry and Chemical Engineering, California Institute of Technology, Pasadena, CA, USA

Peng Liu

Laboratoire de Physique des Solides - UMR 8502, CNRS, Universit\'e Paris-Saclay, 91405 Orsay, France

William Stuart Fall, Henricus H. Wensink

Laboratory for Bio- and Nano-Instrumentation, Institute of Bioengineering, School of Engineering, EPFL, Lausanne, Switzerland

Marcos Penedo Garcia and Georg Fantner

Contributions

Michael Mayer, Alessandro Ianiro and Nico Bruns conceived and supervised this work. Philip B. V. Scholten and Peng Liu synthesized the block copolymers. Christian C. M. Sproncken and Justin Monney prepared and characterized the block copolymer membranes. Brian Van Bueren performed the dry SPM measurements. Carolina Pierucci prepared the membranes for the liquid-phase SPM characterization and helped with the control experiments. Alessandro Ianiro performed the SCF

computations. William S. Fall and Henricus H. Wensink performed the Molecular dynamics simulations. Marcos Penedo Garcia and Georg Fantner performed the LPSPM characterization. Ulrich Steiner and Christoph Weder provided support with data analysis and interpretation. All authors contributed to the writing of the manuscript.

Corresponding authors

Alessandro Ianiro (alessandro.ianiro@unifr.ch) and Michael Mayer (michael.mayer@unifr.ch).

Supplementary Information

Extended data figures 1-4, Supplementary Methods, Supplementary Discussions 1-7, Supplementary Table 1, Supplementary Figures 1-29, Supplementary Video 1.